

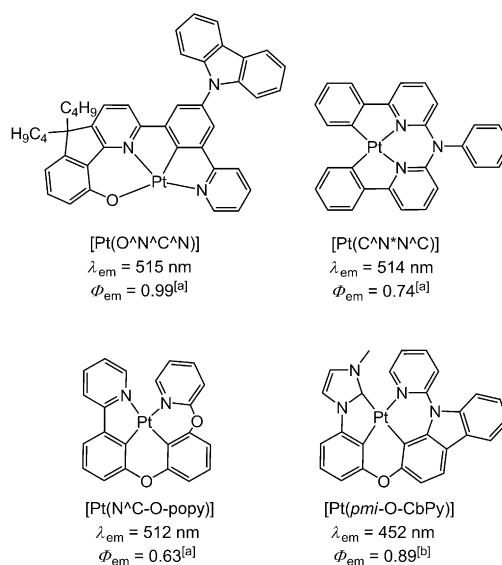
Luminescent Pincer Platinum(II) Complexes with Emission Quantum Yields up to Almost Unity: Photophysics, Photoreductive C–C Bond Formation, and Materials Applications**

Pui-Keong Chow, Gang Cheng, Glenna So Ming Tong, Wai-Pong To, Wai-Lun Kwong, Kam-Hung Low, Chi-Chung Kwok, Chensheng Ma, and Chi-Ming Che*

Abstract: Luminescent pincer-type Pt^{II} complexes supported by C-deprotonated π -extended tridentate R–C[^]N[^]N–R' ligands and pentafluorophenylacetylide ligands show emission quantum yields up to almost unity. Femtosecond time-resolved fluorescence measurements and time-dependent DFT calculations together reveal the dependence of excited-state structural distortions of [Pt(R–C[^]N[^]N–R')(C \equiv C–C₆F₅)] on the positional isomers of the tridentate ligand. Pt complexes [Pt(R–C[^]N[^]N–R')(C \equiv C–Ar)] are efficient photocatalysts for visible-light-induced reductive C–C bond formation. The [Pt(R–C[^]N[^]N–R')(C \equiv C–C₆F₅)] complexes perform strongly as phosphorescent dopants for green- and red-emitting organic light-emitting diodes (OLEDs) with external quantum efficiency values over 22.1 %. These complexes are also applied in two-photon cellular imaging when incorporated into mesoporous silica nanoparticles (MSNs).

Luminescent metal complexes which display strongly emissive, long-lived excited states play an important role in photocatalysis,^[1] luminescence sensing and cellular imaging,^[2] and in phosphorescent organic light-emitting diode (OLED) devices.^[3] While numerous methods and synthetic design strategies to achieve triplet excited states with tunable energies and lifetimes in the microsecond time domain have been established, examples of luminescent metal complexes

with phosphorescence quantum yields (Φ_{em}) close to unity are rare.^[4,5] As the factors governing competitive radiative decay and nonradiative decay of excited states are not well understood, new examples of highly luminescent metal complexes are instrumental in probing the effects of the metal ion and ligand structure on excited-state dynamics. Highly emissive metal complexes, such as the Pt^{II} complexes reported herein, typically contain ligands with a rigid scaffold and strong donor atoms to minimize excited-state structural distortions.^[6] In this regard, luminescent cyclometalated Pt^{II} complexes supported by tetradentate ligands, such as O[^]N[^]C[^]N, C[^]N[^]N[^]C, N[^]C–O–popy, and pmi–O–CbPy (Scheme 1) with high Φ_{em} values, have been developed.^[5,7] These rigid, robust tetradentate ligands are prepared by multistep copper/palladium-catalyzed cross-coupling reactions, making structural modification to suit different purposes a challenging task.



Scheme 1. Pt^{II} complexes supported by tetradentate ligands. [a] Measured in CH₂Cl₂ solution. [b] Measured in a PMMA (poly(methylmethacrylate)) film.

Luminescent Pt^{II} complexes bearing tridentate pincer-type ligands display rich photophysical and photochemical properties. For example, [Pt(N[^]C[^]N)(X)] (N[^]CH[^]N = 1,3-di(2-pyridinyl)benzene; X = Cl, σ -alkynyl)^[6a,c] and [Pt(C[^]N[^]C)(CN*t*Bu)] (HC[^]N[^]CH = 3,6-bis(*p*-anizolyl)-2-carboranyl-pyridine)^[6c] display high Φ_{em} (up to 0.82) in

[*] Dr. P.-K. Chow, Dr. G. Cheng, Dr. G. S. M. Tong, Dr. W.-P. To, W.-L. Kwong, Dr. K.-H. Low, Dr. C.-C. Kwok, Dr. C. Ma, Prof. Dr. C.-M. Che

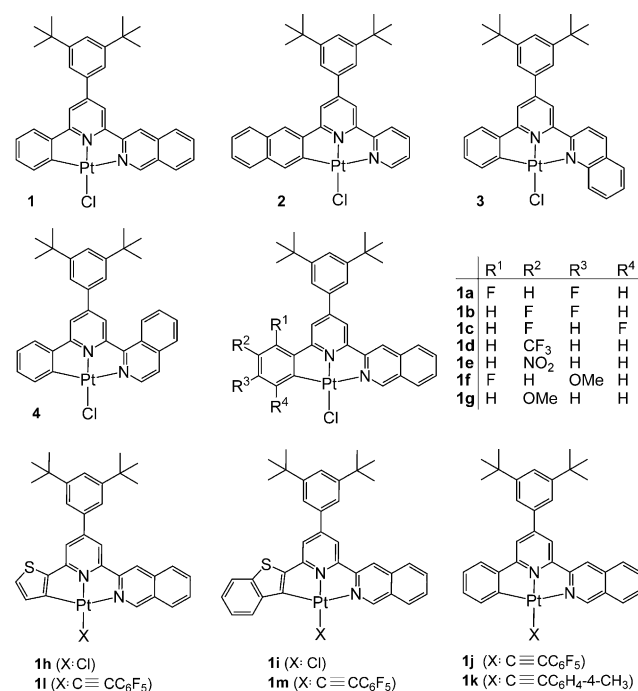
State Key Laboratory of Synthetic Chemistry
Institute of Molecular Functional Materials
HKU-CAS Joint Laboratory on New Materials
Department of Chemistry, The University of Hong Kong
Pokfulam Road, Hong Kong (P.R. China)
E-mail: cmche@hku.hk

Prof. Dr. C.-M. Che
HKU Shenzhen Institute of Research and Innovation
Shenzhen 518053 (China)

[**] This work was supported by the Hong Kong Research Grants Council (HKU 700812P), the CAS-Croucher Foundation Funding Scheme for Joint Laboratories, the Area of Excellence Program (AoE/P-03/08), the National Key Basic Research Program of China (2013CB834802), and the Guangdong Special Project of the Introduction of Innovative R&D Teams, China. We are thankful for the assistance of The University of Hong Kong Li Ka Shing Faculty of Medicine Faculty Core Facility for use of the laser scan confocal microscope.

Supporting information for this article is available on the WWW under <http://dx.doi.org/10.1002/anie.201408940>.

solutions at room temperature and their emission energy could be tuned from $\lambda_{\text{em}} = 471$ to 610 nm.^[6a,c] Herein, we describe a series of highly emissive Pt^{II} complexes supported by C-deprotonated R-C^{^N}N^{^N}-R' ligands with extended π -conjugation (Scheme 2). These complexes show strong phos-



Scheme 2. Chemical structures of the synthesized Pt^{II} complexes [Pt(R-C^{^N}N^{^N}-R')X].

phorescence with Φ_{em} close to unity in some cases and are highly efficient catalysts for visible-light-induced reductive C–C bond formation. The strongly light-emitting materials also have useful applications in high-performance OLEDs and two-photon cellular imaging.

Details of the synthesis and characterization of the Pt^{II} complexes **1–4** and **1a–1m** (Scheme 2) are given in the Supporting Information. The single-crystal X-ray structures of **3** and **1h** have been determined (see Figure S1 and Table S1–S3 in the Supporting Information). The Pt atom in each of these two structures adopts a distorted square-planar coordination geometry. In **3**, the C_{phenyl}–Pt–N_(2-quinoline) angle measures 160.3(2)° and in **1h** the C_{thiophene}–Pt–N_(3-isoquinoline) angle measures 162.6(4)°, respectively. The Pt–N_{pyridine}, Pt–N_(2-quinoline), and Pt–N_(3-isoquinoline) bond lengths (1.970(4)–2.214(4) Å) and Pt–C_{phenyl} (1.989(6) Å) distances are comparable to that of [Pt(C^{^N}N^{^N})(X)] (X = Cl, PPh₃ or μ -dppm).^[8]

The UV/Vis absorption spectra of [Pt(R-C^{^N}N^{^N}-R')Cl] show intense absorption bands at $\lambda = 250$ –350 nm with molar absorptivities (ϵ) on the order of 10^4 dm³ mol^{−1} cm^{−1} and weaker absorption bands at $\lambda = 400$ –470 nm with ϵ values on the order of 10^3 dm³ mol^{−1} cm^{−1} (Figure 1 and Figures S2–S4). The high-energy and low-energy bands are assigned to ¹IL (singlet intraligand) $\pi \rightarrow \pi^*$ and ¹IL/¹MLCT (¹MLCT = singlet metal-to-ligand charge transfer) transitions, respectively. The acetylide-containing complexes **1j–m** show similar absorption bands to those of their chloride precursors **1**, **1h**, and **1i** but

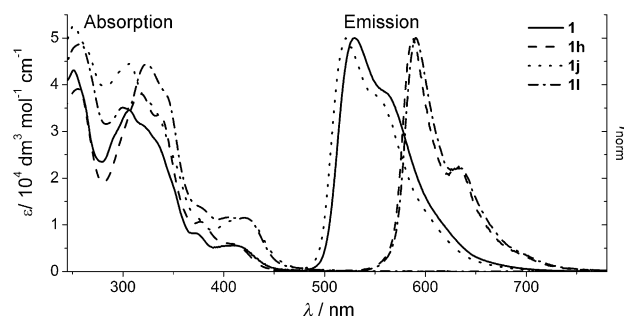


Figure 1. UV/Vis absorption and emission spectra of **1**, **1h**, **1j**, and **1l** in CH₂Cl₂ (2×10^{-5} mol dm^{−3}) at 298 K.

with the lowest-energy absorption band maxima (λ_{max}) red-shifted (Figure 1 and Figure S5 in the Supporting Information). The spectra of **1–4** are different, with the lowest-energy λ_{max} value undergoing a red shift from $\lambda = 416$ nm (**1**) to 439 nm (**2**) to 464 nm (**3**) to 472 nm (**4**) (see Figure S2).

These Pt^{II} complexes are highly emissive, having emission wavelength maxima (λ_p) at $\lambda = 521$ –653 nm, emission lifetimes (τ) between less than 0.2 and 10 μ s, and Φ_{em} values up to approximately 0.99 in CH₂Cl₂ at room temperature (see Figure 1 and Table 1, and Figure S2–S5 and Table S4 in the

Table 1: Photophysical properties of complexes **1–3** and **1h–1k** obtained from fs-TRF and steady-state emission measurements.

	λ_f [nm] ^[a]	τ_f [ps] ^[a]	λ_p [nm] ^[b]	τ_p [μ s] ^[b]	Φ_{em}	k_r [s ^{−1}]	k_{nr} [s ^{−1}]
1	440	0.05	530	7.6	0.78	1.0×10^5	2.9×10^4
2	460	0.06	561	0.7	0.10	1.4×10^5	1.3×10^6
3	410	0.04	624	< 0.2	< 0.001	— ^[c]	— ^[c]
1h	440	0.05	588	10.1	0.25	2.5×10^4	7.5×10^4
1i	440	0.06	644	4.5	0.033	7.3×10^3	2.2×10^5
1j	455	0.10	521	5.5	0.99	1.8×10^5	— ^[d]
1k	— ^[e]	— ^[e]	573	3.5	0.27	— ^[e]	— ^[e]

[a] Data obtained using fs-TRF. [b] Data obtained using steady-state emission measurement. [c] Cannot be determined because of instrumental limitations in the determination of τ_p (< 0.2 μ s). [d] Value too low to be reported. [e] Not determined.

Supporting Information). According to the time-dependent DFT (TDDFT) calculations (Table 2; Table S5), the emission of [Pt(R-C^{^N}N^{^N}-R')Cl] complexes are assigned to excited states with mixed ³MLCT ($d\pi \rightarrow \pi^*_{(\text{R-C}^{\text{^N}}\text{N}^{\text{^N}}\text{-R}^{\text{'}})}$)/ILCT/XLCT ($p\pi_{\text{Cl}} \rightarrow \pi^*_{(\text{R-C}^{\text{^N}}\text{N}^{\text{^N}}\text{-R}^{\text{'}})}$) parentages (ILCT = intraligand charge transfer; XLCT = halogen-to-ligand charge transfer) whereas that of [Pt(R-C^{^N}N^{^N}-R')(acetylide)] have mixed ³MLCT/ILCT/LLCT (LLCT = ligand-to-ligand charge transfer; $\pi_{\text{C}\equiv\text{CAr}} \rightarrow \pi^*_{(\text{R-C}^{\text{^N}}\text{N}^{\text{^N}}\text{-R}^{\text{'}})}$) contributions.^[8c] Notably, the Φ_{em} of **1** is much higher than that of **2–4**, where complexes **2–4** are the structural isomers of **1** with the π -conjugated fragment at different positions of the R-C^{^N}N^{^N}-R' ligand (Φ_{em} : 0.78 (**1**); 0.1 (**2**); < 0.001 (**3**), < 0.001 (**4**)). Complexes **1j**, **1l**, and **1m**, which contain the pentafluorophenylacetylide ligand, show similar emission maxima (± 10 nm) but with at least a twofold increase in Φ_{em} value when compared with that of their chloride precursors **1**, **1h**, and **1i**, respectively. Importantly, **1j**

Table 2: TDDFT calculations on **1j** and **1k** at their respective optimized T_1 excited state.^[a,b]

	Major Contribution	Pt	isoQ	Py2	Ph	C \equiv C	Ar
1j	H \rightarrow L (40%) H-3 \rightarrow L (15%)	15 \rightarrow 5 (-10%)	19 \rightarrow 39 (+20%)	19 \rightarrow 44 (+25%)	16 \rightarrow 5 (-11%)	16 \rightarrow 2 (-14%)	14 \rightarrow 5 (-9%)
1k	H \rightarrow L (41%) H-3 \rightarrow L (18%)	14 \rightarrow 5 (-9%)	17 \rightarrow 41 (+24%)	18 \rightarrow 43 (+25%)	14 \rightarrow 4 (-10%)	18 \rightarrow 2 (-16%)	19 \rightarrow 4 (-15%)

[a] Values in parentheses in the second column indicate the percentage contribution of the transition.

[b] IsoQ = isoquinolinyl moiety; Py2 = central pyridinyl moiety; Ph = cyclometalated phenyl moiety; Ar = substituted phenyl ring at C \equiv C. H: HOMO, L: LUMO.

has a Φ_{em} value near unity, which is the highest among the reported pincer-type Pt^{II} complexes^[6] and is comparable to that of [Pt(O[^]N[^]C[^]N[^])] ($\Phi_{em} \approx 0.99$).^[5a] Complex **1k**, having a 4-methylphenylacetylide ligand, shows a red-shifted emission band with much lower Φ_{em} value relative to **1** (**1k**: $\lambda_p = 573$ nm; $\Phi_{em} = 0.27$, Table 1). All these findings reveal the importance of the structure of both the R-C[^]N[^]N[^]-R' and ancillary ligands on the photophysical properties of this class of Pt^{II} complexes.

The findings of femtosecond time-resolved fluorescence (fs-TRF) measurements (excitation at $\lambda = 350$ nm) and fitted fluorescence decay profiles at selected emission wavelengths for complexes **1–3** and **1h–j** are given in the Supporting Information (Figure S6). All of the complexes show fluorescence decay with time constants close to or less than 0.1 ps revealing very rapid intersystem crossing from the photo-generated singlet to triplet excited states with rate constants $k_{isc} > \approx 10^{13}$ s⁻¹ and quantum yields (Φ_{isc}) of approximately 0.99. Considering this result and the other photophysical properties determined by fs-TRF (λ_f and τ_f) and steady-state emission measurements (λ_p , τ_p , Φ_{em} ; Table S4 in the Supporting Information), the radiative and nonradiative rate constants (k_r and k_{nr}) were estimated (Table 1). Values of k_r fall within the range of circa 1.8×10^5 s⁻¹ (**1j**) to 7.3×10^3 s⁻¹ (**1i**) and k_{nr} values have a range of 1.3×10^6 s⁻¹ (**2**) to approximately 2.9×10^4 s⁻¹ (**1**). Thus, in addition to the relatively high k_r value, the Φ_{em} of **1j** approaching unity is mainly attributed to its negligibly small k_{nr} value. On the other hand, the low Φ_{em} values of **2** and **1i** are attributable mainly to their fast k_{nr} value, and the slow k_r in **1i** also contributes to its low Φ_{em} value.

DFT/TDDFT calculations were performed to address the different photophysical properties among: a) positional isomers having different quinolinyl moieties (**1**, **3**, and **4**); b) structural isomers with different sites of extended π -conjugation (**1** and **2**); and c) complexes containing different ancillary ligands (**1**, **1j**, and **1k**).

Considering first the positional isomers, the optimized ground-state (S_0) and lowest triplet-excited-state (T_1) geometries of complexes **1**, **3**, and **4** are depicted in Figure S7. The R-C[^]N[^]N[^]-R' ligand adopts a coplanar geometry in both the S_0 and T_1 states of **1** and in the S_0 state of **3**, but is significantly distorted (from coplanar geometry) in the T_1 state of **3** and in

both the S_0 and T_1 states of **4**. The distortions can be attributed to electronic repulsion between the hydrogen atom on the 2-quinolinyl moiety and the Cl⁻ ligand in the T_1 state of **3** and also the steric strain between the H atom on the central pyridine ring and the 1-isoquinolinyl moiety in the S_0 state of **4**. The more flexible ligand skeleton of **4** allows the complex to have large structural distortion on going from the S_0 state to the T_1 excited state, resulting in significantly decreased emission quantum yield.

Next, the structural isomers (complexes **1** and **2**) were considered. The T_1 excited state of **2** is mainly composed of HOMO \rightarrow LUMO/LUMO + 1/LUMO + 3 transitions (HOMO = highest occupied molecular orbital; LUMO = lowest unoccupied molecular orbital) whereas that of **1** involves mixed contributions of HOMO-1 \rightarrow LUMO, HOMO-2 \rightarrow LUMO/LUMO + 1, and HOMO \rightarrow LUMO transitions (see Table S5 and Figure S8). The changes in charge density upon going from the S_0 state to the T_1 state are listed in Table S5. As a result of the dominant contributions of the HOMO to the T_1 excited state of **2**, there is a significant drop in charge density (> 40%) at the naphthyl moiety and thus considerable ³ILCT character in the T_1 excited state. In contrast, there are only moderate changes in the charge density on each moiety of **1** (< 25%) and this complex has mixed ³MLCT/¹ILCT/¹XLCT character. The larger ILCT character in the emissive excited state of **2** leads to more significant structural distortion of the C=C/C=N moieties of the cyclometalated ligand. This structural distortion is reflected from the larger Huang–Rhys factor (S_M) computed for normal modes between 1000 and 1500 cm⁻¹ ($S_M = 1.56$ for **1** and 1.86 for **2**), thereby resulting in a faster nonradiative decay rate.

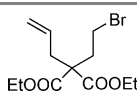
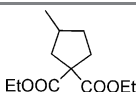
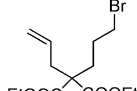
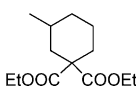
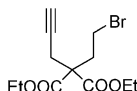
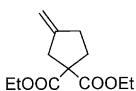
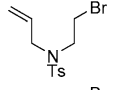
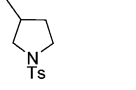
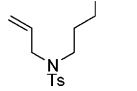
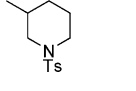
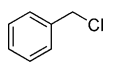
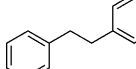
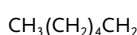
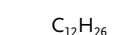
Finally, the effect of the ancillary ligand, involving specifically complexes **1**, **1j**, and **1k**, is considered. Compared with the chloride ligand (in **1**), for **1j** with the pentafluorophenylacetylide ligand a substantial decrease in the nonradiative decay rate was found, whereas for **1k**, employing the 4-methylphenylacetylide ligand, the nonradiative decay rate was found to increase. This can be accounted for by the change in the order of frontier molecular orbitals on going from **1** to **1j/1k**: the Pt(d_{xz}) orbital coupled with the π (C \equiv CAr) and π (central pyridyl) orbitals now becomes the HOMO in **1j** and **1k** (see Figure S9); the LUMO is essentially localized on the central pyridyl and the isoquinolinyl moieties of the R-C[^]N[^]N[^]-R' ligand. The T_1 excited states of **1j** and **1k** are mainly derived from HOMO \rightarrow LUMO and HOMO-3 \rightarrow LUMO transitions, that is, they are mainly of ³LLCT character ($\pi_{C\equiv CAr} \rightarrow \pi^*_{(R-C^N N-R')}$) with less influence of the ³MLCT and ³ILCT characters than in the T_1 state of **1**. (Note: ³ILCT occurs between the phenyl and the isoquinolinyl moieties of the R-C[^]N[^]N[^]-R' ligand, denoted as $\pi_{phenyl} \rightarrow \pi^*_{isoquinolinyl}$; please see Table 2 for the TDDFT results

and the change in charge density of **1j** and **1k** at their respective optimized T_1 geometries). The decrease in ILCT character leads to less structural distortion along the aromatic C=C/C=N normal stretching modes of the cyclometalated ligand as reflected from the smaller S_M in **1j** and **1k** ($S_M = 1.25$ for **1j** and 1.39 for **1k**). However, with the more electron-donating 4-methylphenylacetylide ligand, the HOMO of **1k** is more destabilized than that of **1**, leading to a smaller energy gap between the T_1 and S_0 states. Moreover, the phenylacetylide ligand has a larger contribution in the HOMO of **1k** (37%) than in the HOMO of **1j** (30%). Therefore, there are larger bond-length changes in the Pt-C≡CAr moiety in **1k** than in **1j**. For example, the changes in the C≡C and C≡C-C fragments are +0.025 and -0.033 Å, respectively, for **1k** but +0.019 and -0.019 Å for **1j**. The consequence for the smaller structural distortion in **1j** renders the high-frequency C=C and C≡C stretching modes to be less effective energy acceptors in **1j** than in **1k**. Therefore, the combined energy-gap effect and the smallest structural distortion along the high-frequency normal modes render **1j** to have the slowest nonradiative decay rate among the complexes studied.

This class of Pt^{II} complexes are powerful photoreductants or photooxidants which can be excited by visible light. As an example, **1j** shows strong absorption at wavelengths between $\lambda = 400$ –450 nm; its excited state is both a strong oxidant (estimated $E(\mathbf{1j}^*/\mathbf{1j}^-) = 0.65$ V) and a powerful reductant ($E(\mathbf{1j}^+/\mathbf{1j}^*) = -2.40$ V versus $\text{Cp}_2\text{Fe}^+/\text{Cp}_2\text{Fe}^0$; see the Supporting Information).

The visible-light-induced reductive cyclization of alkyl bromides has been examined. In the presence of diisopropylethylamine ($i\text{Pr}_2\text{NEt}$) as a sacrificial electron donor in CH_3CN and using a blue LED as the light source ($\lambda_{\text{em}} = 420$ –520 nm, $\lambda_{\text{max}} = 462$ nm, see the Supporting Information), alkyl bromides **A**¹–**E**¹ gave the cyclized products with conversions and yields of up to 99% and 78%, respectively, after 4–8 hours of irradiation (entries 1, 3–6, Table 3). This photocatalysis has been extended to benzyl chloride and 1-bromohexane (entries 7 and 9, Table 3). Under similar reaction conditions, the conversion and yield for the reaction of benzyl chloride were 87% and 39% respectively. However, the product yield of the reaction of 1-bromohexane was only about 1.5%. Control experiments in the absence of **1j** (entries 2, 8, and 10, Table 3) showed no product formation under similar conditions, except a product yield of 0.2% determined from the benzyl chloride experiment by NMR spectroscopy (entry 9, Table 3). Reduction of C–X bonds to produce carbon-centered radical intermediates is an important step in organic transformation.^[9] Emission quenching experiments revealed that the excited state of **1j** is quenched by $i\text{Pr}_2\text{NEt}$ but not substrate **B**¹, following Stern–Volmer behavior with a k_q value (quenching rate constant) of $5.80 \times 10^9 \text{ mol}^{-1} \text{ dm}^3 \text{ s}^{-1}$. Nanosecond transient absorption (ns-TA) spectroscopy experiments were performed with CH_3CN solutions containing **1j**, and **1j** and $i\text{Pr}_2\text{NEt}$ (Figure S13 and S14). The time-resolved absorption difference spectra recorded at different delay times after a $\lambda = 355$ nm laser pulse excitation of a solution containing **1j** and $i\text{Pr}_2\text{NEt}$ (Figure S14) showed the formation of **1j**[−] with an absorption maximum band at $\lambda_{\text{max}} \approx 354$ nm and ≈ 700 nm that are

Table 3: Photoinduced C–C bond formation of alkyl/benzyl halide.

		$\text{A}^1\text{--G}^1 \xrightarrow[\text{CH}_3\text{CN, blue LED, 4–8 h, 25 } ^\circ\text{C}]{\text{a) or b)}} \text{A}^2\text{--G}^2$			
Entry	Cat.	Substrate	Product	Conv.; Yield [%]	
1 ^[a,d]	1j			> 99; 78 ^[g]	
2 ^[c,d]	–	–	–	0; 0 ^[g]	
3 ^[a,f]	1j			> 99; 77 ^[g]	
4 ^[a,e]	1j			> 99; 57 ^[g]	
5 ^[b,d]	1j			87; 57 ^[g]	
6 ^[b,f]	1j			83; 49 ^[g]	
7 ^[a,d]	1j			87; 39 ^[g]	
8 ^[c,d]	–	–	–	< 1; 0.2 ^[g]	
9 ^[a,d]	1j			–; 1.5 ^[h]	
10 ^[c,d]	–	–	–	0; 0 ^[h]	

[a] Procedure a: **1j** (1 mol %), $i\text{Pr}_2\text{NEt}$ (2 equiv), CH_3CN . [b] Procedure b: **1j** (1 mol %), $i\text{Pr}_2\text{NEt}$ (5 equiv), HCO_2H (2 equiv), CH_3CN . [c] Procedure a without the addition of **1j**. [d], [e], [f] The reaction mixture was irradiated for 4, 5, 8 hours, respectively. [g] Determined by ^1H NMR spectroscopy. [h] Determined by gas chromatography. [i] Not determined. Ts = tosylate.

reminiscent of the absorption spectrum of the one-electron-reduced $[\text{Pt}(\text{N}^{\wedge}\text{N}^{\wedge}\text{N})(\sigma\text{-alkynyl})]$ complex ($\text{N}^{\wedge}\text{N}^{\wedge}\text{N} = 4,4',4''\text{-tri-}t\text{-butyl-2,2':6',2''\text{-terpyridine}}$) which has $\lambda_{\text{max}} \approx 360$ nm and ≈ 770 nm.^[10] The formation of **1j**[−] is also in line with the estimated driving force (ΔE) of +0.32 V for the electron-transfer reaction between the excited state of **1j** and $i\text{Pr}_2\text{NEt}$ (see the Supporting Information). The electron-transfer reaction of **1j**[−] and benzyl chloride (or **B**¹) can be revealed from the cyclic voltammograms of the mixture of **1j** and benzyl chloride (or **B**¹) in dimethylformamide (DMF; 0.1 mol dm^{−3} $n\text{Bu}_4\text{NPF}_6$ as the electrolyte; Figure S16). Upon addition of benzyl chloride (or **B**¹) the reversible couple (**1j**/**1j**[−]) was replaced by an irreversible cathodic wave with enhanced current attributed to the reduction of benzyl chloride by the electrogenerated **1j**[−].

Although the radical cyclization reactions of alkyl/aryl halides with Ru^{II} and Ir^{III} sensitizers have been reported, the reported examples were confined to substrates containing activated or weak carbon–halogen bonds such as polyhalomethane, electron-deficient benzyl halides, and alkyl/aryl iodide.^[9] A recent report with $[\text{Au}_2(\mu\text{-dppm})_2]\text{Cl}_2$ as photocatalyst showed that even substrates having unactivated C–Br bonds can undergo radical cyclization.^[11] However, $[\text{Au}_2(\mu\text{-dppm})_2]\text{Cl}_2$ only shows strong absorption in the high-energy UV spectral region with very weak to no absorption at

wavelengths greater than $\lambda = 350$ nm.^[11] In this work, by using the Pt^{II} catalyst **1j**, we have demonstrated that the radical cyclization of substrates with unactivated C–Br bonds can take place using visible light as light source.

In view of their high emission quantum yields, this class of Pt^{II} complexes was examined as phosphorescent OLED dopant materials. Four monochromatic OLEDs I–IV based on **1**, **1h**, **1j**, and **1l**, respectively, and with a configuration of ITO/TAPC(50 nm)/TCTA:Pt^{II} complex (x %, 10 nm)/TmPyPB (50 nm)/LiF (1 nm)/Al (100 nm) were fabricated and characterized. In these devices, ITO is indium tin oxide, TAPC is 4,4'-cyclohexylidenebis[*N,N*-bis(4-methylphenyl)-benzamine] (used as the hole-transporting material), TCTA is 4,4',4''-tri(9-carbazoyl)triphenylamine (used as the host material), and TmPyPB is 3,3'-[5'-[3-(3-pyridinyl)phenyl][1,1':3',1''-terphenyl]-3,3''-diyl]bispyridine (used as the electron-transporting material). The performance data of the devices are summarized in Table S6. Complexes **1**, **1h**, **1j**, and **1l** were doped into TCTA with optimized concentrations as the light-emitting material. Normalized electroluminescence (EL) spectra of the devices are depicted in Figure 2a. The EL emission maxima of the devices are slightly red-shifted (3–10 nm) from that of the photoluminescence of the metal complexes in solution at room temperature. Devices I and III showed yellowish-green emission with CIE coordinates of

(0.431, 0.557) and (0.368, 0.598), respectively. Saturated red emission with CIE coordinates of (0.610, 0.380) and (0.628, 0.367) were recorded for devices II and IV. In all these cases, emission from the host material at approximately $\lambda = 400$ nm was not detected, indicating complete energy transfer from TCTA to the dopant. The maximum current efficiencies of the devices were in the range of 23.1–76.7 cd A^{−1} (Table S6). Figure 2b depicts the EQE–current-density curves (EQE = external quantum efficiency) for devices I–IV. The maximum EQE of 22.8 % shown by device III is among the highest values recently reported with phosphorescent Pt^{II} dopant materials.^[5,7] Moreover, the saturated red-emitting device II showed a high EQE of 22.1 %, which is comparable to that of best red-emitting devices based on Ir^{III} complexes.^[12]

We examined the application of **1j** in cellular imaging. For the delivery of **1j** to cancer cells and to overcome its low solubility in aqueous medium, **1j**-encapsulated mesoporous silica nanoparticles (**1j**@MSNs) were prepared with characterization data given in the Supporting Information. MSNs have been established as suitable nanovehicles for cellular delivery of therapeutic or diagnostic reagents.^[13] Herein, MCM-41-type MSNs with an average diameter of 160 nm were used. Human epithelial cervical carcinoma (HeLa) cells were treated with **1j**@MSNs (300 $\mu\text{g mL}^{-1}$) and fluorescence imaging experiments revealed that **1j** was successfully uptaken by the HeLa cells, as shown in Figure 3. The cytosolic

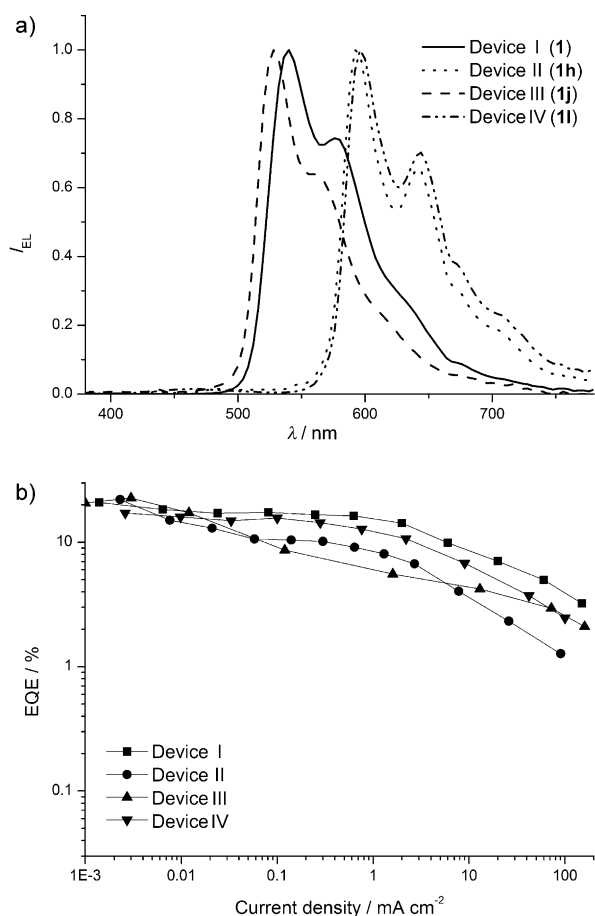


Figure 2. a) Normalized EL spectra and b) external quantum efficiency (EQE) versus current density characteristics for devices I–IV.

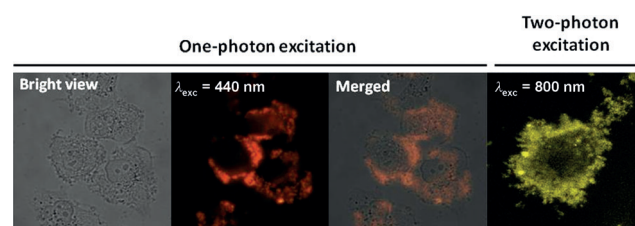


Figure 3. Images of HeLa cells treated with **1j**@MSNs (300 $\mu\text{g mL}^{-1}$) by one-/two-photon excitation microscopy. For one-photon fluorescence imaging, $\lambda_{exc} = 440$ nm and a long pass emission filter > 590 nm was used. For two-photon imaging, $\lambda_{exc} = 800$ nm and the fluorescence was collected at $\lambda = 520$ –600 nm.

puncta localization pattern is attributed to entrapment of MSNs in endosomes after uptake by endocytosis which is a commonly recognized uptake mechanism of MSNs into mammalian cells.^[14] Complex **1j** displays two-photon-induced emission properties (with a two-photon cross section measuring approximately 17 GM at $\lambda = 756$ nm, Figure S18). Upon excitation with a laser at $\lambda = 800$ nm, the emission of **1j** in the cytosol, which is highly similar to that obtained by one-photon excitation, was clearly detected in HeLa cells treated with **1j**-loaded MSNs. With appropriate surface modifications of MSNs by attachment of tumor-specific ligands, we anticipate that applications of MSNs loaded with [Pt(R–C^{^N}^N–R')] complexes could be used in the field of cancer diagnostics.

In conclusion, a series of pincer-type [Pt(R–C^{^N}^N–R')] complexes with emission quantum yields approaching unity were prepared using ligand systems with easily modifiable structures. Both R–C^{^N}^N–R' and ancillary ligands have

a significant effect on the excited-state structural distortion. This class of complexes are effective photocatalysts for visible-light-induced reductive C–C bond formation of benzyl chloride/unactivated alkyl bromides. Their high emission quantum yields render them to be good phosphorescent dopant materials leading to high performance green- and red-emitting OLEDs with highest EQEs of 22.8% and 22.1%, respectively, achieved. Encapsulating **1j** in MSNs for two-photon-excited cellular imaging has been demonstrated.

Received: September 9, 2014

Published online: January 9, 2015

Keywords: density functional calculations · luminescence · organic light-emitting diodes · photochemistry · platinum

- [1] a) A. J. Esswein, D. G. Nocera, *Chem. Rev.* **2007**, *107*, 4022–4047; b) J. L. Dempsey, B. S. Brunschwig, J. R. Winkler, H. B. Gray, *Acc. Chem. Res.* **2009**, *42*, 1995–2004; c) W. T. Eckenhoff, R. Eisenberg, *Dalton Trans.* **2012**, *41*, 13004–13021; d) D. M. Schultz, T. P. Yoon, *Science* **2014**, *343*, 1239176.
- [2] a) K. M.-C. Wong, V. W.-W. Yam, *Acc. Chem. Res.* **2011**, *44*, 424–434; b) E. Baggeley, J. A. Weinstein, J. A. G. Williams, *Coord. Chem. Rev.* **2012**, *256*, 1762–1785; c) M. Mauro, A. Aliprandi, D. Septiadi, N. S. Kehr, L. De Cola, *Chem. Soc. Rev.* **2014**, *43*, 4144–4166.
- [3] a) S.-W. Lai, C.-M. Che, *Top. Curr. Chem.* **2004**, *241*, 27–63; b) P. I. Djurovich, M. E. Thompson in *Highly Efficient OLEDs with Phosphorescent Materials* (Ed.: H. Yersin), Wiley-VCH, Weinheim, **2008**, pp. 131–161; c) H. Yersin, A. F. Rausch, R. Czerwieniec, T. Hofbeck, T. Fischer, *Coord. Chem. Rev.* **2011**, *255*, 2622–2652; d) P.-T. Chou, Y. Chi, M.-W. Chung, C.-C. Lin, *Coord. Chem. Rev.* **2011**, *255*, 2653–2665; e) L. Xiao, Z. Chen, B. Qu, J. Luo, S. Kong, Q. Gong, J. Kido, *Adv. Mater.* **2011**, *23*, 926–952.
- [4] a) Y. Kawamura, K. Goushi, J. Brooks, J. J. Brown, H. Sasabe, C. Adachi, *Appl. Phys. Lett.* **2005**, *86*, 071104; b) T. Sajoto, P. I. Djurovich, A. B. Tamayo, J. Oxgaard, W. A. Goddard III, M. E. Thompson, *J. Am. Chem. Soc.* **2009**, *131*, 9813–9822.
- [5] a) G. Cheng, P.-K. Chow, S. C. F. Kui, C.-C. Kwok, C.-M. Che, *Adv. Mater.* **2013**, *25*, 6765–6770; b) E. Turner, N. Bakken, J. Li, *Inorg. Chem.* **2013**, *52*, 7344–7351.
- [6] a) J. A. G. Williams, *Chem. Soc. Rev.* **2009**, *38*, 1783–1801; b) A. F. Rausch, L. Murphy, J. A. G. Williams, H. Yersin, *Inorg. Chem.* **2012**, *51*, 312–319; c) E. Rossi, A. Colombo, C. Dragonetti, D. Roberto, R. Ugo, A. Valore, L. Falciola, P. Brulatti, M. Cocchi, J. A. G. Williams, *J. Mater. Chem.* **2012**, *22*, 10650–10655; d) P.-K. Chow, W.-P. To, K.-H. Low, C.-M. Che, *Chem. Asian J.* **2014**, *9*, 534–545; e) A. M. Prokhorov, T. Hofbeck, R. Czerwieniec, A. F. Suleymanova, D. N. Kozhevnikov, H. Yersin, *J. Am. Chem. Soc.* **2014**, *136*, 9637–9642.
- [7] a) D. A. K. Vezzu, J. C. Deaton, J. S. Jones, L. Bartolotti, C. F. Harris, A. P. Marchetti, M. Kondakova, R. D. Pike, S. Huo, *Inorg. Chem.* **2010**, *49*, 5107–5119; b) X.-C. Hang, T. Fleetham, E. Turner, J. Brooks, J. Li, *Angew. Chem. Int. Ed.* **2013**, *52*, 6753–6756; *Angew. Chem.* **2013**, *125*, 6885–6888.
- [8] a) W. Lu, B.-X. Mi, M. C. W. Chan, Z. Hui, C.-M. Che, N. Zhu, S.-T. Lee, *J. Am. Chem. Soc.* **2004**, *126*, 4958–4971; b) S. C. F. Kui, I. H. T. Sham, C. C. C. Cheung, C.-W. Ma, B. Yan, N. Zhu, C.-M. Che, W.-F. Fu, *Chem. Eur. J.* **2007**, *13*, 417–435; c) M. L. Clark, S. Diring, P. Retailleau, D. R. McMillin, R. Ziessel, *Chem. Eur. J.* **2008**, *14*, 7168–7179; d) J. Schneider, P. Du, P. Jarosz, T. Lazarides, X. Wang, W. W. Brennessel, R. Eisenberg, *Inorg. Chem.* **2009**, *48*, 4306–4316; e) M.-Y. Yuen, S. C. F. Kui, K.-H. Low, C.-C. Kwok, S. S.-Y. Chui, C.-W. Ma, N. Zhu, C.-M. Che, *Chem. Eur. J.* **2010**, *16*, 14131–14141.
- [9] a) J. D. Nguyen, E. M. D’Amato, J. M. R. Narayanam, C. R. J. Stephenson, *Nat. Chem.* **2012**, *4*, 854–859; b) H. Kim, C. Lee, *Angew. Chem. Int. Ed.* **2012**, *51*, 12303–12306; *Angew. Chem.* **2012**, *124*, 12469–12472.
- [10] E. Shikhova, E. O. Danilov, S. Kinayyigit, I. E. Pomestchenko, A. D. Tregubov, F. Camerel, P. Retailleau, R. Ziessel, F. N. Castellano, *Inorg. Chem.* **2007**, *46*, 3038–3048.
- [11] G. Revol, T. McCallum, M. Morin, F. Gagosz, L. Barriault, *Angew. Chem. Int. Ed.* **2013**, *52*, 13342–13345; *Angew. Chem.* **2013**, *125*, 13584–13587.
- [12] C.-L. Ho, H. Li, W.-Y. Wong, *J. Organomet. Chem.* **2014**, *751*, 261–285.
- [13] S.-H. Wu, C.-Y. Mou, H.-P. Lin, *Chem. Soc. Rev.* **2013**, *42*, 3862–3875.
- [14] I. Slowing, B. G. Trewyn, V. S.-Y. Lin, *J. Am. Chem. Soc.* **2006**, *128*, 14792–14793.